Astronomy & Astrophysics manuscript no.
(will be inserted by hand later)

A study of infrared recombination lines in Herbig Ae/Be stars *

M.E. van den Ancker[1,2], F. Fortuin[3], and L.B.F.M. Waters[3,4]

[1] Harvard-Smithsonian Center for Astrophysics, 60 Garden Street, MS 42, Cambridge MA 02138, USA
[2] European Southern Observatory, Karl-Schwarzschild-Str. 2, 85748 Garching bei München, Germany
[3] Astronomical Institute, University of Amsterdam, Kruislaan 403, 1098 SJ Amsterdam, The Netherlands
[4] Instituut voor Sterrenkunde, Katholieke Universiteit Leuven, Celestijnenlaan 200B, B-3001 Heverlee, Belgium

Received <date>; Accepted <date>

Abstract. We present a study of the circumstellar environment of 26 Herbig Ae/Be stars using infrared H I recombination line observations made by the short wavelength spectrometer onboard the *Infrared Space Observatory* (ISO). A total of 15 different H I transitions have been observed. Our sources mostly showed infrared (IR) H I lines in the Brackett, Pfund and Humphreys series. A comparison of the measured H I line strengths to those predicted by the Storey & Hummer (1995) case B line recombination model showed that the strength of the lines from low-lying transitions (before Pfδ) are not in agreement with case B. We conclude that these lines must be (partially) optically thick. Possible structures in the circumstellar environment that can produce these optically thick lines are a stellar wind or circumstellar disk. From the correlation between the optical Hα and IR Brα line strength we conclude that the principal IR line emission is coming from a compact region close to the central star. This rules out an extended source, such as a H II region. The majority of sources have a double-peaked Hα line profile from which we conclude that the emitting gas is situated in a rotating geometry. This is a strong indication of the presence of a circumstellar disk. The limited correlation between the Brα line strength and stellar UV luminosity leads us to the conclusion that besides the central star, another source of energy must be present to power the IR recombination lines.

Key words. Circumstellar matter – Stars: emission-line – Stars: pre-main-sequence – Stars: winds, outflows – Infrared: stars

1. Introduction

The circumstellar environment of Herbig Ae/Be stars has a complex geometry which is still not well understood. Although during early phases of core collapse the presence of a roughly spherical envelope is generally accepted, the presence of a circumstellar disk in later evolutionary phases has long been a matter of debate. Recent high angular resolution imaging at sub-millimeter wavelengths of several Herbig Ae/Be stars (see Mannings & Sargent 1997) has shown that these stars indeed possess compact (several 100 AU) disks. However it is possible that a low-density envelope is still present. In addition, some Herbig Ae/Be stars are also believed to have outflows. It is important to establish the geometry of the circumstellar environment of Herbig Ae/Be stars, since this is closely related to the evolution of the star and its proto-planetary system.

This paper aims to contribute to our understanding of the circumstellar environment of Herbig Ae/Be stars by studying infrared (IR) H I emission lines in a sample of 26 HAeBes observed by the *Infrared Space Observatory* (ISO). A first question that needs to be answered is what is the source of the IR H I lines? Possible candidates are an (extended) H II region illuminated by a bright UV source, a wind or a circumstellar disk. There are several diagnostic tools available to discern between these structures. Also we check if the picture we get from these IR lines is confirmed by optical and radio observations.

The remainder of this paper is organized as follows: Section 2 describes the observational IR data we used, how the data was reduced and what methods we applied. The resulting data set is described in section 3. This set is complemented by a set of optical and radio literature data. In section 4 we analyze our data by deploying various diagnostic tools. Section 5 discusses the validity of the results and ends with some concluding remarks.

Send offprint requests to: M.E. van den Ancker (mvandenancker@cfa.harvard.edu)

* Based on observations with ISO, an ESA project with instruments funded by ESA Member States (especially the PI countries: France, Germany, the Netherlands and the United Kingdom) and with the participation of ISAS and NASA.

2. ISO Observations

Data for 25 Herbig stars were obtained with the Short Wavelength Spectrometer (SWS; de Graauw et al. 1996) on board the *Infrared Space Observatory* (ISO; Kessler et al. 1996) as part of two guaranteed time ISO-SWS programs (P.I. P. Wesselius and C. Waelkens). Because of the limited sensitivity of the SWS, only sources that are relatively bright at infrared wavelengths (at least a few Jy in the near-infrared) were selected. The sample of stars we looked at was selected using the definition for Herbig Ae/Be stars as described by Waters & Waelkens (1998), but also includes several F-type stars. Sources were selected from literature lists of Herbig Ae/Be stars (Thé et al. 1994; Malfait et al. 1998). The selection yielded 25 stars. With T Tauri added for reference to the less massive counterparts of Herbig Ae/Be stars, the total number of stars in the sample becomes 26.

A list of all stars and their basic parameters can be found in Table 1. Here the position at which the telescope was pointed and an ID number is given to each source for quick identification in plots. Of the 26 stars in our sample most are associated with one or more larger structures. 14 stars are found in a dark cloud, 14 in a bright nebula and 15 in a stellar aggregate. Only 5 stars seem to be isolated. The distance of the sources ranges between 80 and 1050 pc, with 70% of sources within the 100–300 pc range. Of all stars, six are known to be part of a binary system. The spectral type of most stars is Ae or Be as defined by the Herbig Ae/Be selection criterion. However five stars are early Fe stars. T Tau is not a Herbig Ae/Be star and is multiple system, whose primary component has spectral type K0–1e.

The SWS instrument provides spectroscopy between 2.38 and 45.2 micron with a spectral resolving power ($\lambda/\Delta\lambda$) between 900 and 2500. There are many H I lines available in this wavelength range. Between 2 and 12 micron the first lines of the first few line series (Brackett, Pfund, Humphreys) can be found. These lines have the highest probability of being detected because they are expected to be the strongest and because the signal to noise ratio of the SWS is optimal in this range. However, the longer wavelength region also contains several intrinsically strong lines which one might detect in selected sources. The list of lines which were selected for study in this paper are listed in Table 2. For most objects, most of the lines in the SWS wavelength range were scanned with the full grating resolution (observing mode "AOT 02" or "AOT 06"), although in some objects the data were taken from lower resolution full grating scans ("AOT 01").

Data were reduced in a standard fashion using calibration files corresponding to ISO off-line processing software (OLP) version 7.0, after which they were corrected for remaining fringing and glitches. To increase the S/N in the final spectra, detectors were aligned and statistical outliers were removed, after which the data for each object were combined into one final rebinned spectrum.

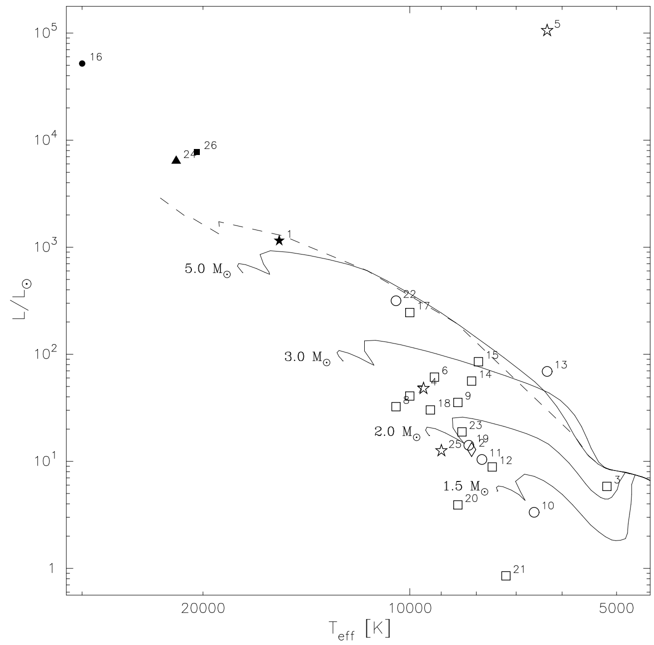

Fig. 1. Hertzsprung-Russell Diagram (HRD) of the 26 stars in our sample. The symbols stand for different Hα profiles (□: double-peaked, ∘: single-peaked, ⋆: P Cygni, △: complex, ⋄: unknown), using open and closed symbols to denote the spectral type (open: B6 or later, closed: B5 or earlier). The solid and dashed lines are the pre-MS evolutionary tracks and the birthline from Bernasconi (1996). The ID numbers correspond to the numbers in Table 1.

Line fluxes were measured by first selecting a small region of the spectrum centered around the rest wavelength of the line. Subsequently, a local continuum is defined by fitting a polynomial of power 1 (a straight line) to two spectral intervals adjacent to the line. If this did not give a proper fit result (e.g. if the line sits on top of a broad solid-state feature), the power of the polynome was varied. After subtraction of this local continuum, line fluxes were determined by integrating the spectrum over an interactively selected wavelength interval. Because the lines have a velocity dispersion that is small compared to the dispersion by the instrumental profile (c.f. Fig. 2), all lines have a nearly gaussian profile dictated by instrumental properties. Therefore no information on the line widths could be derived from our ISO data.

If no line could be discerned, we estimated an upper limit to the flux value by computing the flux for a line with a width dictated by the instrumental profile, and a peak flux of 3 times the noise measured at the position of the line. The error in the values measured is caused partly due to noise in the line and continuum, and partly due to the photometric calibration of the ISO SWS instrument. The latter contribution to the error is usually the greater. The errors used in the remainder of this paper include both contributions.

Measured lines and upper limits are listed in Table 3. 15 out of 22 IR H I lines were detected at at least 1 source. Seven of the lines listed in Table 2 were not detected in

Table 1. Astrophysical Parameters of sample stars. The ID numbers are used to identify sources in various plots. The positions (R.A. and Declination) are the coordinates of the ISO pointing for each source. d stands for the distance to the star (or association to which it belongs). The Hα column gives the Hα profile: S(ingle-peaked), D(ouble-peaked), P(Cygni profile), C(omplex profile) or U(nknown). When more than one value for the Hα equivalent width (EW) was found, both are listed (e.g. −15.7, −21.7). The visual magnitude A_V, effective temperature $T_{\rm eff}$ and luminosity $L_\star$ were obtained from van den Ancker et al. (1998), or calculated for sources not in that paper using the method described there. The masses and ages are estimated using the pre-main sequence evolutionary tracks (Bernasconi 1996) plotted in the HR diagram (Fig. 1).

Source	ID #	α (2000)	δ (2000)	Region	d [pc]	Ref.	Spectral Type	Ref.	Hα	Ref.	EW(Hα) [Å]	Ref.	A_V [$^{\rm m}$]	$\log T_{\rm eff}$	$\log L_\star/L_\odot$	$L_{\rm abs}$ [$L_\odot$]	$L_{\rm emm}$ [$L_\odot$]	Mass [$M_\odot$]	log(age) [yr]
V376 Cas	1	00 11 26.6	+58 50 04	Cas R1	630	(1)	B5e	(11)	P	(27)	−33.4	(41)	8.24	4.19	3.06	1140	6.23	5.2(4)	5.6(3)
Elias 3-1	2	04 18 40.6	+28 19 17	L 1495	160	(2)	A6:e	(12)	U		−29.3	(31)	7.83	3.91	1.11	10.9	10.9	1.9(1)	6.7(1)
T Tau	3	04 21 59.1	+19 32 06	Tau R2	140	(3)	K1e+M:	(13)	D	(28)	−38.0	(42)	1.18	3.71	0.77	21.4	26	2.4(3)	6.0(3)
AB Aur	4	04 55 45.7	+30 33 06	Tau R2	140	(4)	A0Ve+sh	(14)	P	(29)	−41.2	(43)	0.50	3.98	1.68	2.84	3.0	2.7(3)	6.4(2)
Z CMa	5	07 03 43.2	−11 33 06	CMa R1	1050	(5)	F6IIIe	(4)	P	(28)	−20.5	(31)	2.42	3.80	5.02	105000	520	–	–
HD 95881	6	11 01 57.7	−77 30 50		280	(6)	A2III-IVe	(15)	D	(30)	−14.4	(31)	0.53	3.96	1.79	27.7	33.4	2.7(3)	6.4(2)
HD 97048	7	11 08 04.6	−77 39 17	Cha I	180	(4)	B9–A0ep+sh	(16)	D	(28)	−48.7	(28)	1.24	4.00	1.61	31.8	10.3	2.7(3)	6.5(2)
HD 100546	8	11 33 25.8	−70 11 41	DC296.2-7.9	103	(4)	B9Vne	(15)	D	(30)	−29.0	(31)	0.28	4.02	1.51	10.7	21.8	2.3(3)	6.9(2)
HD 104237	9	12 00 05.8	−78 11 34	Cha III	116	(4)	A4IVe+sh	(4)	D	(31)	−23.2	(31)	0.31	3.93	1.55	9.86	25.4	2.3(3)	6.4(2)
HD 135344	10	15 15 48.4	−37 09 15		80	(6)	F4Ve	(17)	S	(31)	−14.4	(17)	0.31	3.82	0.52	0.72	2.3	1.2(2)	7.2(3)
HD 139614	11	15 40 46.5	−42 29 52	Sco OB2?	160	(6)	A7Ve	(17)	S	(32)	−6.69	(17)	0.09	3.90	1.02	0.936	9.47	1.7(2)	6.8(1)
HD 142666	12	15 56 40.1	−22 01 39	Sco OB2?	120	(6)	A8Ve	(17)	D	(32)	−3.23	(17)	0.93	3.88	0.95	4.8	4.05	1.7(2)	6.9(1)
HD 142527	13	15 56 41.9	−42 19 22	Anon.	200	(4)	F7IIIe	(4)	S	(33)	−17.9	(31)	1.49	3.80	1.84	40.8	40.8	3.5(6)	5.8(4)
HD 144432	14	16 06 58.1	−27 43 08	Sco R1	290	(6)	A5Ve	(4)	D	(32)	−9.00	(17)	0.56	3.91	1.75	19.4	36.9	2.7(3)	6.4(2)
HR 5999	15	16 08 34.2	−39 06 18	Lupus 3	210	(4)	A5–7IIIe+sh	(18)	D	(34)	−5.52	(31)	0.47	3.90	1.93	30.4	55.1	3.2(5)	5.8(4)
CD−42°11721	16	16 59 06.8	−42 42 08	DC343.3-0.6	1000	(6)	B0IVep	(19)	S	(35)	−199.5	(31)	5.05	4.48	4.72	51900	51900	>10	–
51 Oph	17	17 31 24.9	−23 57 44	Sco OB2?	131	(4)	B9.5Vne	(20)	D	(31)	−2.99	(31)	0.15	4.00	2.39	48	48	4.0(5)	5.8(3)
HD 163296	18	17 56 21.4	−21 57 20		122	(4)	A3Ve	(21)	D	(36)	−15.7, −21.7	(44)	0.25	3.97	1.48	3.38	22	2.3(3)	6.5(2)
HD 169142	19	18 24 29.9	−29 46 48	Sco OB2?	140	(6)	A5Ve	(17)	S	(37)	−14.0	(17)	0.43	3.91	1.15	4.99	9.14	1.9(1)	6.7(1)
R CrA	20	19 01 53.9	−36 57 10	NGC 6729	130	(7)	A1e–F7e var	(4)	D	(28)	−24.5	(31)	1.64	3.93	0.59	2.97	0.944	1.5(5)	7.6(4)
T CrA	21	19 01 58.8	−36 57 49	NGC 6729	130	(7)	F0e	(22)	D	(28)	−5.51	(31)	2.45	3.86	−0.07	0.67	0.18	1.0(8)	–
HD 179218	22	19 11 11.2	+15 47 17	L693	240	(4)	B9e	(23)	S	(31)	−18.5	(31)	1.27	4.02	2.50	244	71.1	4.3(5)	5.7(3)
WW Vul	23	19 25 58.6	+21 12 31	Vul R1	440	(8)	A4IV–Ve+sh	(21)	D	(38)	−25.2, −40.9	(38)	0.96	3.92	1.28	9.97	8.86	1.9(1)	6.8(2)
BD+40°4124	24	20 20 28.3	+41 21 51	Cyg R1	1000	(9)	B2Ve	(24)	C	(39)	−31.8, −100.7	(41,39)	3.16	4.34	3.81	6320	75.3	10(2)	–
PV Cep	25	20 45 54.0	+67 57 36	Cep R2	440	(10)	A5:e	(25)	P	(25)	−40, −200	(25)	7.01	3.95	1.10	12.1	0.43	1.8(2)	7.2(2)
HD 200775	26	21 01 36.8	+68 09 49	Cep R2	440	(10)	B2.5IVe	(26)	D	(40)	−30, −104	(45)	1.92	4.31	3.89	7400	286	10(2)	4.2(3)

References: (1) Shevchenko & Yakubov (1989); (2) Kenyon et al. (1994); (3) Elias (1978); (4) van den Ancker et al. (1998); (5) Shevchenko et al. (1999); (6) Main-sequence distance (adopted); (7) Marraco & Rydgren (1981); (8) Voshchinnikov (1981); (9) Shevchenko et al. (1991); (10) Whitcomb et al. (1981); (11) Cohen & Kuhi (1979); (12) Zinnecker & Prebisch (1994); (13) Maihara & Kataza (1991); (14) Böhm & Catala (1993); (15) Houk & Cowley (1975); (16) Whittet et al. (1987); (17) Dunkin et al. (1997); (18) Tjin A Djie et al. (1989); (19) Shore et al. (1990); (20) Abt & Morrell (1995); (21) Gray & Corbally (1998); (22) Finkenzeller & Mundt (1984); (23) Slettebak (1966); (24) Hillenbrand et al. (1995); (25) Cohen et al. (1981); (26) Rogers et al. (1995); (27) Corcoran & Ray (1998); (28) Reipurth et al. (1996); (29) Böhm & Catala (1995); (30) Grady et al. (1996); (31) M.E. van den Ancker, unpublished data; (32) Meeus et al. (1998); (33) Pérez & Grady (1997); (34) Praderie et al. (1991); (35) de Winter & Thé (1990); (36) Pogodin (1994); (37) Dunkin et al. (1997b); (38) Pugach (1988); (39) Férnandez et al. (1997); (40) Beskrovnaya et al. (1994); (41) Corcoran & Ray (1998); (42) Cohen & Kuhi (1980); (43) Böhm & Catala (1997); (44) Baade & Stahl (1989); (45) Miroshnichenko et al. (1998).

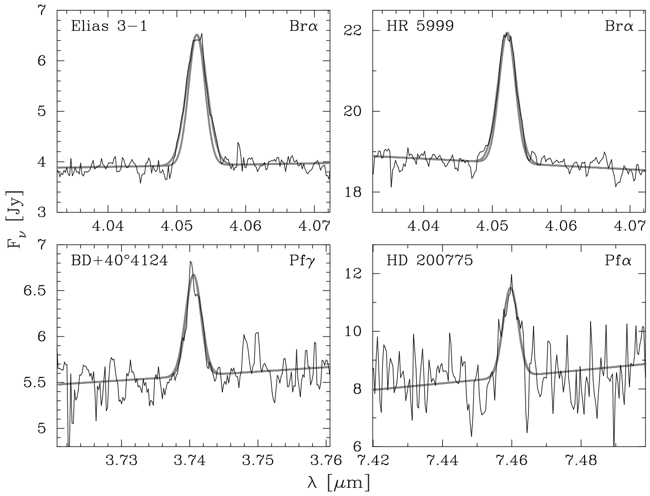

Fig. 2. Examples of detected lines in our sample. Note the close match between instrumental profile (grey lines) and the observed data (solid), indicating that these lines are not resolved.

any of the sources. These were Huβ, Huδ, H7α, H7β, H7δ, H8α, H8β, H9α and H9β. They have been omitted from Table 3.

3. Resulting Data Set

3.1. Measured Lines & Upper Limits

The measured flux has been absorbed and scattered by dust in the line of sight. This material can be both circumstellar and interstellar. We correct the flux for extinction, based on the assumption that the line of sight to the H I emitting region has the same extinction as the line of sight to the central star, using the visual extinction values (A_V) towards the central star listed in Table 1 and the extinction curve derived by Fluks et al. (1994). Note that by using the Fluks et al. extinction curve we assume the circumstellar extinction to have the same wavelength dependence as that of the interstellar medium. Strictly speaking this may not be correct, since the grain population of the dust that causes the extinction in star forming regions is likely different from that in the diffuse interstellar medium. However, since the extinction correction applied to the infrared lines is small, we do not expect this to significantly affect our results.

The flux is also corrected for the distance of the source, so all sources can be compared on absolute figures as well as relative figures. The correction involves multiplying the measured flux by the surface of a sphere with radius d: $F' = F \times 4\pi d^2$, with d the distance (in meters) to the star as listed in Table 1. For every line that was detected in at least one source we complemented the detection(s) with upper limit determinations in the remaining lines. The upper limits are also corrected for extinction and distance.

The resulting data-set of intrinsic IR H I line fluxes can be found in Table 3. The detected luminosity values for individual lines range between about 2.0×10^{22} and 2.5×10^{26} W.

Table 2. Examined Lines in Programme Stars. The transition numbers denote between which energy levels n the line is produced. The wavelength is measured in vacuum. Note that Huβ and H7δ are blended at the ISO-SWS resolving power, i.e. only their combined contribution to the line flux can be measured.

Line	Transition	λ [μm]	Beam Size [$''$]
Brackett series			
Brα	5–4	4.05226	14×20
Brβ	6–4	2.62587	14×20
Pfund series			
Pfα	6–5	7.45986	14×20
Pfβ	7–5	4.65378	14×20
Pfγ	8–5	3.74056	14×20
Pfδ	9–5	3.29699	14×20
Pfϵ	10–5	3.03920	14×20
Pf11	11–5	2.87300	14×20
Pf12	12–5	2.75827	14×20
Humphreys series			
Huα	7–6	12.37221	14×27
Huβ	8–6	7.50829	14×20
+H7δ	11–7	7.50268	14×20
Huγ	9–6	5.90821	14×20
Huδ	10–6	5.12866	14×20
Huϵ	11–6	4.67251	14×20
Hu14	14–6	4.02087	14×20
Hansen-Strong Series			
H7α	8–7	19.06190	14×27
H7β	9–7	11.30870	14×20
H8 series			
H8α	9–8	27.80338	20×27
H8β	10–8	16.20910	14×20
H9 series			
H9α	10–9	38.87082	20×33
H9β	11–9	22.34046	14×27

3.2. Literature Data

More definite conclusions about the circumstellar environment of our programme stars can be drawn by supplementing our IR line data-set with optical and radio data. Hα is the strongest recombination line available in ground based optical observations. Information about the Hα (H I 3–2) line profiles and equivalent widths (EWs) of our programme stars was collected from literature and is listed in Table 1. In our sample there are six sources with a single-peaked Hα profile, 14 sources with double-peaked profile, four sources with P Cygni profiles and one source for which no information on the Hα profile is available in the literature.

In some cases a star was mentioned in different papers with different values for the equivalent width or Hα profile.

Table 3. Extinction corrected absolute (distance independent) line-luminosities of programme stars measured using ISO-SWS. All values are luminosities in Watts.

Source	No.	Brα	Brβ	Huα	Huγ	Huε	Hu 14
V376 Cas	1	< 4.49e+24	< 9.33e+24	< 1.71e+25	< 1.99e+25	< 1.16e+25	< 2.93e+25
Elias 3-1	2	4.91(0.59)e+23	5.56(1.22)e+23	–	–	–	< 2.14e+22
T Tau	3	2.62(1.11)e+23	4.83(0.88)e+23	< 3.98e+23	< 5.46e+23	< 1.14e+23	2.31(1.30)e+23
AB Aur	4	8.59(1.27)e+23	8.01(0.75)e+23	< 9.68e+23	< 1.01e+24	< 6.63e+23	< 1.26e+24
Z CMa	5	< 6.98e+25	< 5.36e+25	< 2.11e+26	< 2.60e+26	< 1.23e+26	< 1.94e+26
HD 95881	6	4.31(0.29)e+23	1.32(0.15)e+24	< 2.53e+24	< 2.59e+24	< 2.40e+24	< 5.84e+24
HD 97048	7	7.59(0.36)e+23	5.09(0.52)e+23	< 7.09e+23	< 2.17e+23	< 1.97e+23	< 4.35e+23
HD 100546	8	4.66(0.13)e+23	6.49(0.22)e+23	< 2.53e+23	< 1.58e+23	< 1.12e+23	< 1.62e+23
HD 104237	9	3.12(0.11)e+23	3.41(0.17)e+23	< 1.44e+24	< 1.12e+24	< 1.27e+24	< 2.75e+24
HD 135344	10	< 1.13e+23	< 2.20e+23	< 5.01e+23	< 6.14e+23	< 5.34e+23	< 1.41e+24
HD 139614	11	< 2.30e+22	< 3.59e+22	< 2.88e+23	< 1.52e+23	< 1.66e+23	< 1.72e+23
HD 142666	12	< 1.67e+22	< 3.18e+22	< 6.66e+22	< 1.17e+23	< 7.57e+22	< 1.52e+23
HD 142527	13	< 9.11e+23	< 1.21e+24	< 4.76e+24	< 4.08e+24	< 2.41e+24	< 5.89e+24
HD 144432	14	< 4.94e+23	< 6.18e+23	< 9.94e+23	< 1.26e+24	< 8.10e+23	< 1.3e+24
HR 5999	15	7.37(0.73)e+23	–	–	–	< 4.44e+23	–
CD−42°11721	16	2.11(0.13)e+26	2.46(0.11)e+26	1.83(0.18)e+26	2.71(0.31)e+25	2.40(0.41)e+25	2.88(0.14)e+25
51 Oph	17	4.47(0.14)e+23	< 4.47e+23	< 8.01e+23	< 8.23e+23	< 4.80e+23	< 8.13e+23
HD 163296	18	4.04(0.50)e+23	9.91(0.84)e+23	< 3.97e+23	< 3.92e+23	< 4.16e+23	< 6.42e+23
HD 169142	19	< 3.71e+23	< 4.75e+23	< 3.29e+24	< 1.53e+24	< 1.37e+24	< 2.28e+24
R CrA	20	< 9.11e+22	1.30(0.14)e+24	< 1.03e+24	< 7.86e+23	< 4.05e+23	< 7.27e+23
T CrA	21	< 1.27e+23	< 2.7e+23	< 8.36e+23	< 5.84e+23	< 1.05e+23	< 2.30e+23
HD 179218	22	< 6.37e+23	< 9.76e+23	< 2.69e+24	< 2.62e+24	< 1.40e+24	< 3.13e+24
WW Vul	23	< 2.76e+24	–	–	–	< 1.33e+24	< 1.86e+24
BD+40°4124	24	3.90(0.12)e+25	3.56(0.19)e+25	< 3.82e+25	< 3.00e+25	< 7.37e+24	4.42(0.49)e+24
PV Cep	25	< 4.44e+24	< 8.24e+24	< 3.45e+25	< 3.23e+25	< 1.19e+25	< 3.31e+25
HD 200775	26	1.46(0.04)e+25	1.56(0.05)e+25	< 6.55e+24	< 6.49e+24	< 2.97e+24	1.56(0.11)e+24

Source	No.	Pfα	Pfβ	Pfγ	Pfδ	Pfε	Pf 11	Pf 12
V376 Cas	1	< 8.10e+24	< 9.56e+24	< 5.96e+24	< 4.78e+24	< 3.92e+24	< 3.88e+24	< 4.32e+24
Elias 3-1	2	–	–	–	–	–	–	–
T Tau	3	< 1.38e+23	< 1.49e+23	< 1.42e+23	< 1.03e+23	< 8.08e+22	< 9.21e+22	< 1.78e+23
AB Aur	4	1.63(0.48)e+23	< 3.69e+23	6.22(0.53)e+23	2.40(0.24)e+23	2.26(0.13)e+23	3.78(0.22)e+23	< 8.60e+23
Z CMa	5	< 1.09e+26	< 1.39e+26	< 4.87e+25	< 3.06e+25	< 3.96e+25	< 3.88e+25	< 4.58e+25
HD 95881	6	< 9.45e+23	< 2.21e+24	< 5.59e+23	< 7.25e+23	< 5.51e+23	< 5.47e+23	< 8.00e+23
HD 97048	7	< 1.3e+23	< 3.45e+23	1.76(0.20)e+23	2.63(0.21)e+23	1.26(0.17)e+23	1.08(0.30)e+23	1.25(0.21)e+23
HD 100546	8	8.68(1.23)e+22	1.92(0.21)e+23	1.36(0.06)e+23	2.01(0.07)e+23	9.63(0.71)e+22	8.24(0.64)e+22	1.46(0.14)e+23
HD 104237	9	< 4.61e+23	< 1.44e+24	< 3.39e+23	< 7.57e+23	< 2.77e+23	< 3.03e+23	< 4.47e+23
HD 135344	10	< 1.76e+23	< 5.00e+23	< 1.42e+23	< 1.68e+23	< 9.52e+22	2.02(0.19)e+22	< 1.71e+23
HD 139614	11	< 5.73e+22	< 1.61e+23	< 4.24e+22	< 2.52e+22	< 3.46e+22	< 3.51e+22	< 3.65e+22
HD 142666	12	< 3.44e+22	< 1.10e+23	< 2.08e+22	< 3.34e+22	< 1.98e+22	< 3.19e+22	< 3.56e+22
HD 142527	13	< 1.65e+24	< 2.57e+24	< 1.45e+24	< 1.21e+24	< 9.41e+23	< 8.57e+23	< 1.49e+24
HD 144432	14	< 3.84e+23	< 6.35e+23	< 2.38e+23	< 2.72e+23	< 2.14e+23	< 2.18e+23	< 2.34e+23
HR 5999	15	< 3.95e+23	< 3.47e+23	2.77(0.59)e+23	–	–	–	–
CD−42°11721	16	2.60(0.27)e+25	5.09(0.49)e+25	5.94(0.26)e+25	6.83(0.31)e+25	6.54(0.20)e+25	8.39(0.23)e+25	6.13(0.25)e+25
51 Oph	17	< 3.58e+23	< 7.28e+23	< 1.61e+23	< 3.41e+23	< 1.89e+23	< 3.32e+23	< 2.58e+23
HD 163296	18	5.90(1.93)e+22	< 1.34e+23	4.63(1.46)e+22	3.49(0.31)e+23	< 1.48e+23	< 1.93e+23	< 1.47e+23
HD 169142	19	< 5.85e+23	< 9.05e+23	< 4.35e+23	< 2.99e+23	< 3.01e+23	< 4.35e+23	< 3.55e+23
R CrA	20	3.56(0.96)e+23	< 5.55e+23	< 8.74e+22	< 1.23e+23	< 7.24e+22	< 6.25e+22	< 2.31e+23
T CrA	21	< 1.17e+23	< 4.19e+23	< 4.17e+22	< 1.09e+23	< 7.79e+22	< 1.08e+23	< 1.56e+23
HD 179218	22	< 1.59e+24	< 1.22e+24	< 3.87e+23	< 8.36e+23	< 2.35e+23	< 4.01e+23	< 4.41e+23
WW Vul	23	< 5.28e+23	< 1.20e+24	< 4.03e+23	–	–	–	–
BD+40°4124	24	5.70(2.09)e+24	1.28(0.32)e+25	1.57(0.05)e+25	1.72(0.08)e+25	1.28(0.12)e+25	8.52(0.75)e+24	1.27(0.09)e+25
PV Cep	25	< 6.00e+24	< 2.15e+25	< 4.50e+24	< 4.04e+24	< 2.76e+24	< 4.69e+24	< 5.25e+24
HD 200775	26	1.88(0.19)e+24	3.17(1.16)e+24	3.27(0.15)e+24	4.63(0.15)e+24	5.03(0.18)e+24	5.13(0.16)e+24	4.57(0.16)e+24

Table 4. Programme star radio flux densities at 3.6 and 6.0 cm from literature.

Source	ID #	$S_{3.6}$ [mJy]	Ref.	$S_{6.0}$ [mJy]	Ref.
Elias 3-1	2	0.48±0.12	(1)	–	
T Tau	3	5.19±0.17	(2)	4.62±0.12	(2)
AB Aur	4	0.123±0.020	(3)	0.119±0.020	(3)
Z CMa	5	2.17±0.93	(4)	–	
HD 97048	7	–		<0.36	(4)
HR 5999	15	<0.10	(4)	–	
CD−42°11721	16	<1.32	(4)	–	
HD 163296	18	0.240±0.042	(5)	0.196±0.034	(5)
R CrA	20	<0.10	(4)	–	
T CrA	21	<0.09	(4)	–	
BD+40°4124	24	0.32±0.15	(4)	0.38±0.27	(4)
PV Cep	25	0.32	(6)	–	
HD 200775	26	0.57±0.26	(4)	–	

References: (1) di Francesco et al. (1997); (2) Skinner & Brown (1994); (3) Güdel et al. (1989); (4) Skinner et al. (1993); (5) van den Ancker et al. (2000); (6) Anglada et al. (1992).

This may be due to either intrinsic variability in the Hα line (e.g. HD 163296; Beskrovnaya et al. 1998) or be due to variations in the continuum (e.g. UX Ori; Grinin et al. 1994). In these cases a range of EW values and the most occurring profile have been listed.

The equivalent width of a line is defined as the width of the continuum (at the wavelength of the line) that produces the same amount of flux as the line itself. If the spectral resolution of the EW measurement is sufficient to discern the EW of the photosphere the Hα, the EW gives us a direct measure of the emission line. In lower spectral resolution data, the measured Hα EW likely includes a contribution due to photospheric Hα absorption, and the latter, obtained from a Kurucz (1991) model atmosphere appropriate for the spectral type of the star, was subtracted before further conversions and corrections were made. To convert the EW to a line flux, we multiplied it by the continuum flux, determined by fitting a Kurucz (1991) model atmosphere to optical spectral energy distribution data. This flux was corrected for distance and extinction following the same procedure as for the measured IR data.

Continuum flux is generated by coulomb interactions between ions and electrons (as opposed to bound-bound transitions that produce lines). In the radio wavelength-region the free-free (collisions of electrons with ions) contribution of H is the dominant source of continuum flux. Therefore further diagnostics of the ionized gas in the circumstellar environment may come from radio continuum measurements of our sample stars (unlike the situation in classical Be stars, the infrared continuum in Herbig Ae/Be stars is generally dominated by thermal emission from dust and therefore cannot be used to probe the ionized gas). Such literature data is listed in Table 4. These data were corrected for distance (there is virtually no extinction at the radio wavelengths) using the same process as used for the measured IR data.

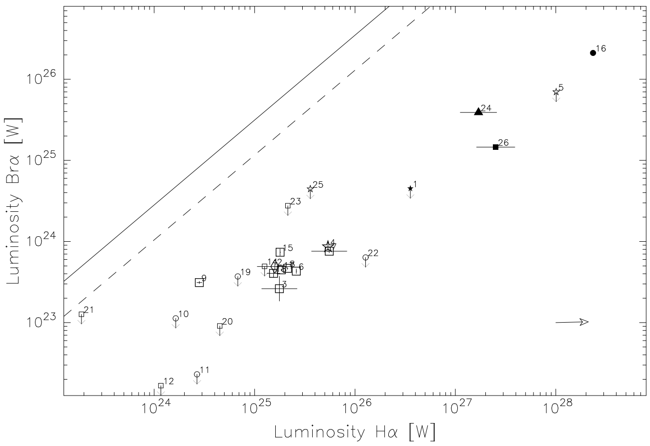

Fig. 3. Correlation between Brα and Hα line strengths. The symbols stand for different Hα profiles (□: double-peaked, ∘: single-peaked, ⋆: P Cygni, △: complex, ⋄: unknown), using open and closed symbols to denote the spectral type (open: B6 or later, closed: B5 or earlier). Smaller symbols with an arrow attached to it stand for upper limit measurements. The solid and dashed lines are respectively the minimum and maximum case B values (see Section 4.3 for the model parameters). The numbers next to each symbol are the ID numbers that correspond to the ID numbers in Table 1. The arrow in the lower right of the plot indicates the direction of interstellar reddening (A_V = 1). Note that the plotted data are absolute (distance independent) values.

4. Analysis

To find what kind of structure is responsible for the observed infrared H I emission lines in Herbig Ae/Be stars, we employ several diagnostic tools. They are discussed individually in the following sub-sections.

4.1. Correlation between IR and Optical Line Strengths

A correlation between the Hα lines found in literature and the measured infrared Brα lines gives information about the location of the gas that emits the lines. Because the spatial resolution in Hα is much higher than the infrared (Hα is measured using a spectrograph with a slit width of typically ∼ 2″, while the ISO-SWS has an aperture of 14″ × 20″), an optical correlation could pinpoint the IR source. Brα is chosen because it is the strongest and most often detected IR H I line available in the sample.

If a correlation between Hα and the infrared lines is found, it is likely that both originate from the same area of the stellar environment. In Fig. 3 the Hα line strength is plotted versus the Brα line strength. All sources have known Hα line fluxes from literature. Thirteen sources were detected in Brα. The plot of Hα vs Brα shows a clear correlation between the two line strengths. From this correlation one can conclude that the optical and infrared emission are coming from the same gas and this must thus be located close to the central star.

4.2. Gas Kinematics

By looking at the shape of the line profile, we can obtain information on the gas dynamics. Because of the typically much higher spectral resolution of optical spectra, the Hα line is best suited for this. Several characteristic profiles can be distinguished: A single peak line profile indicates that the gas is not moving parallel to the line of sight. A double-peaked profile indicates a rotating structure, where one peak is blue-shifted moving towards the observer and one is red-shifted moving away. A third possibility is a P Cygni profile: a blue-shifted absorption profile from gas in front of the central star, that absorbs the intense emission from the star itself. This is combined with an emission profile from the circumstellar gas that is not in the line of sight to the stellar disk.

In Table 1, the sample of 26 stars show 14 double-peaked, six single-peaked and four P Cygni line profiles (the Hα line profile of Elias 3-1 is unknown and BD+40°4124 has a complex line profile). A double-peaked profile points to the presence of a stellar disk and a P Cygni profile could arise from a stellar wind.

4.3. IR Line Ratios

In order to differentiate between dense (e.g. disk-like) structures and less dense (e.g. wind-like) structures we look at the optical depth of the IR lines. The density is closely related to the optical depth. Amongst others, Storey & Hummer (1995) model that predicts line strength ratios for Menzel & Baker (1938) Case B (i.e. optically thin in all lines except Lyα) recombination. Their model did not only take photon interactions into account but also incorporated collisional transitions. This means the model is dependent on the density and the electron temperature. The calculated minimum and maximum values for the line strength ratios using the Storey & Hummer model were obtained by looking at the resulting ratio for different values of both temperature and density. We varied the parameters between 1000–30,000 K and 10^3–10^9 g cm^{-3}. We believe these numbers to span the range of plausible conditions in the environment of young stellar objects.

To see if case B recombination theory applies to our sources, plots were made of the IR line flux ratios (Fig. 4). In the plots we also show the minimum and maximum case B model line ratios for the explored range of the parameter space. The arrow in the lower right of each plot is the reddening arrow. This arrow shows the shift in position a point on the plot would get if the extinction would increase by a factor of 10 magnitudes. If the extinction is underestimated, the plotted points would shift in this direction.

Brackett α is the strongest line and was detected most often. Therefore we start by plotting our distance-corrected line fluxes against Brα (Fig. 4). The line ratios seen in this figure do not match the predictions from the case B model. This could be explained by assuming that the Brα line flux is smaller than expected from case B, indicating that it is not optically thin. To verify this assumption, we also plot each line in the Pfund series against the next line in the series (Pfα vs Pfβ, Pfβ vs Pfγ, etc.). This plot is shown in Fig. 5. For each panel in this figure the agreement with case B becomes somewhat better, until a case B situation is found in the ratios of Pfδ over Pfϵ and beyond.

Based on this ratio plot analysis of the optical depth of the gas we conclude that within our sample, the IR recombination lines start to become optically thin only beyond Pfδ. All others do not agree with case B predictions. The densities in these sources must be quite high to produce (partially) optically thick IR recombination lines. However, the ratio plot diagnostic is a very coarse tool. It uses a large range of luminosities in its plots and a large range of temperatures and densities in its case B models. For the stars in our sample for which we have detected more than three lines, we therefore also apply a more detailed diagnostic, the Curve of Growth analysis.

The infrared line observational Curve of Growth (CoG) is a plot of the IR line flux against an optical depth parameter. This plot is used to study the density structure in the source of the lines. The line strength is expressed in equivalent width (EW) over λ. Dividing the EW by λ ensures the line strength is expressed in a wavelength-independent way. Contrary to popular convention we define the EW of emission lines as a positive value, and take the EW with respect to the stellar continuum:

$$EW = F_{line}/F_{\lambda\star} \tag{1}$$

Here F_{line} is the observed line flux in W m^{-2} (corrected for extinction, distance correction will only result in a shift along the y-axis and was therefore omitted) and $F_{\lambda\star}$ is the stellar continuum flux in W m^{-2} μm^{-1}. At IR wavelengths the wavelength dependence of $F_{\lambda\star}$ is the same as that of a black-body source function: $\sim \lambda^{-4}$. The stellar continuum is chosen in such a way that it is 1 W m^{-2} μm^{-1} at 1 μm:

$$B_\nu(T) \sim \lambda^{-2} \Rightarrow F_{\lambda\star} = C_1\lambda^{-4} \tag{2}$$

C_1 is chosen so that it equals unity. This choice of stellar continuum will not alter the shape of the CoG, only the scaling of the y-axis.

The optical depth parameter X_{line} is taken from Zaal et al. (1995):

$$X_{line} = \nu^{-3}(1 - e^{h\nu/kT})A_{mn}n^2 e^{(\chi_H - \chi_n)/kT} \tag{3}$$

X_{line} is related to the density (n), temperature T, the ionization energy χ, the Einstein A coefficient and the frequency ν. The temperature used for the calculation of X_{line} was 10,000 K. However, the temperature dependence of X_{line} is weak and it only affects the scale on the x-axis, not the shape of the curve.

In general a CoG consists of 3 parts: A linear part that corresponds to gas that is optically thin. This part

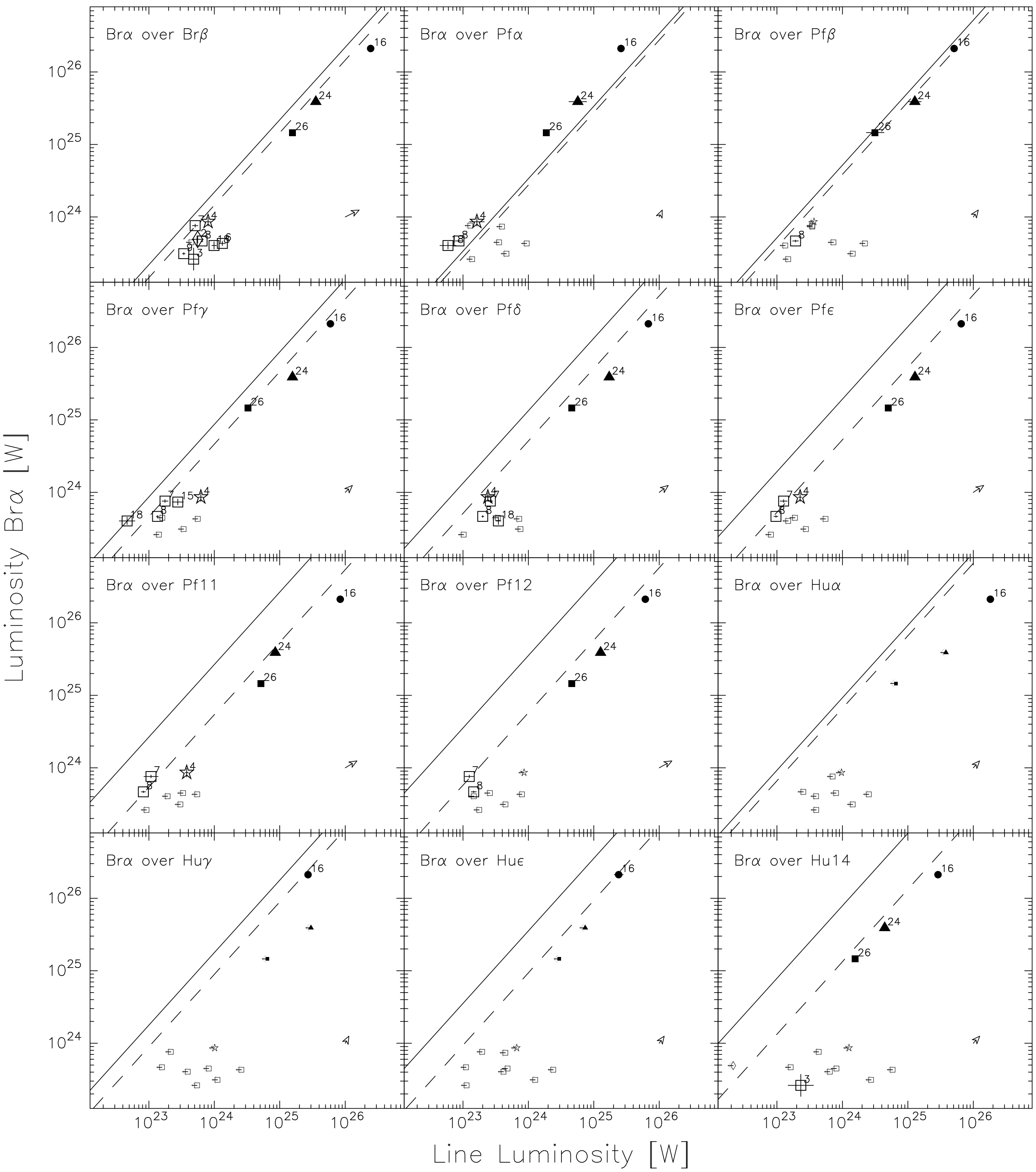

Fig. 4. Brα Line Ratios. Plot symbols have the same meaning as in Fig. 3. The arrow in the lower right of each plot indicated the direction of interstellar reddening ($A_V = 10$). The solid and dashed lines are respectively the minimum and maximum case B values. The numbers next to each symbol are the ID numbers that correspond to the ID numbers in various tables. Note that these data are absolute (distance independent) values.

has a slope of ~1. When there is more material to emit flux, you see all the extra emitted flux. The second part is the intermediate part between the linear and the flat part. In this part the slope of the CoG is dependent on the density structure. The lines of this part are partially optically thick. It is an indication of the density gradient in the source. For an isothermal disk structure the inner part of the structure becomes optically thick while the outer parts still contribute more to the flux when the density increases. The third part is the opaque part. In this

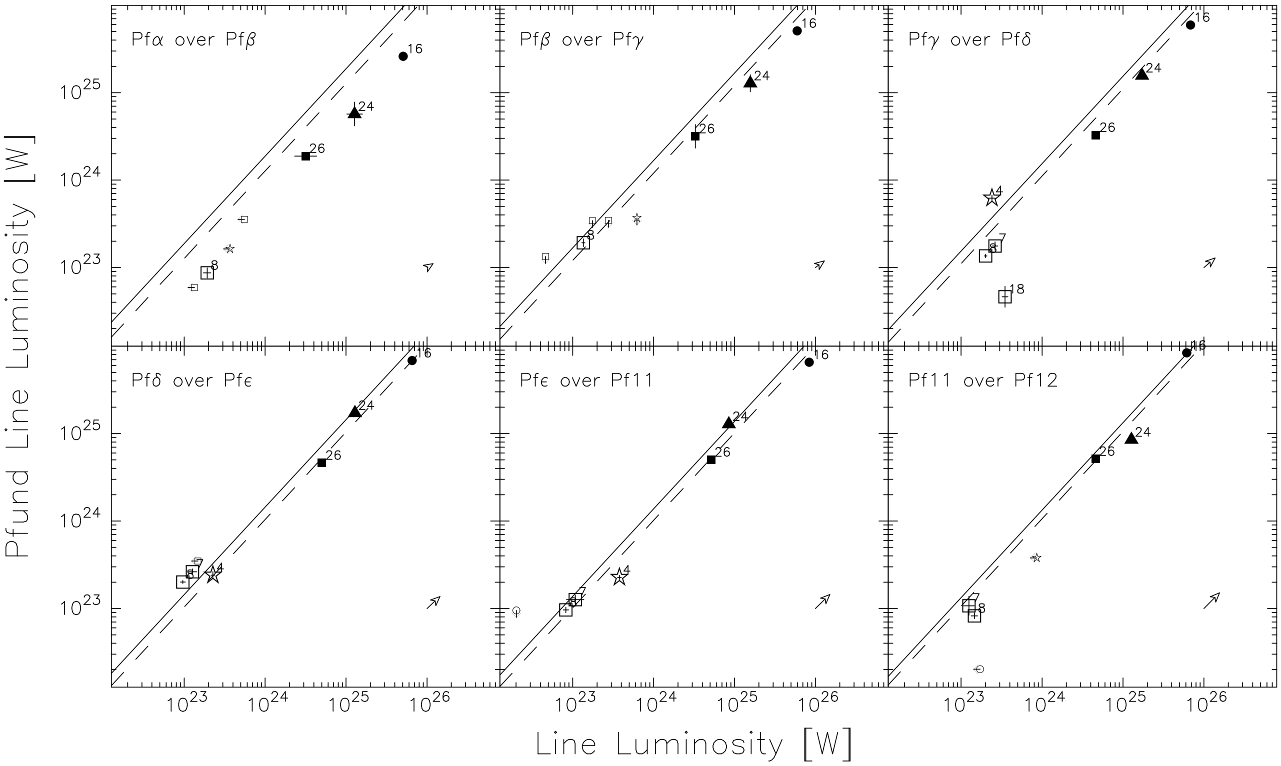

Fig. 5. Pfund Series Line Ratios. Lines, arrows and plot symbols have the same meaning as in Fig. 4.

flat part of the curve the line strength is independent of the opacity. When the optical depth increases there is no increase in received flux. Only the outer layer of the emitting structure is observed. A schematic CoG is plotted in Fig. 6.

This schematic behaviour expected of line strengths as a function of X_{line} can be complicated if more than a single gas component is present. This may be the case for Herbig Ae/Be stars since they are often surrounded by low-density H II regions. We refer the reader to Zaal et al. (1995) and Hony et al. (2000) for more exhaustive descriptions of the IR line CoG method.

For six stars we have enough IR line measurements to construct a CoG. These were BD+40°4124, HD 100546, HD 200775, HD 97048, AB Aur, and CD−42°11721. Their CoGs are plotted in Figs. 7 and 8. In these diagrams, each line series is denoted by a different plot symbol. The source number is printed with the name for easy comparison to other plots and tables. The Pfund series is plotted for each source beginning with the intrinsically strong Pfα on the right, down to the weaker Pf12 on the left. When no line was detected an upper limit is plotted. Since both the x- and y-axis are scaled by an unknown value, we focus our analysis on the slope of the CoG rather than on the absolute values obtained. First we analyze the individual plots and compare them with the results from the line ratio plots.

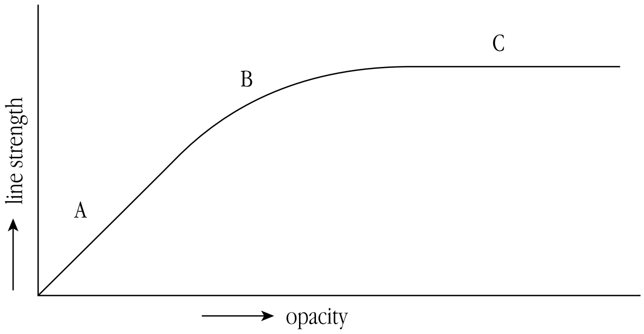

Fig. 6. Schematic Curve of Growth. In part A the lines are optically thin. Part B is the intermediate part where optical depth effects become apparent. The optically thick part (C) shows no dependence on line strength.

BD+40°4124. The leftmost Pfund line is Pf12. It does not show a case B line ratio in the ratio plots. The next three lines from the left (Pf11, Pfϵ and Pfδ) do show case B ratios. The CoG for this star does not appear to form a smooth curve, causing some uncertainties in its interpretation. A linear (slope = 1) part could be present until Pfδ, followed by an intermediate part (with lower slope). However a straight line with a slope less than 1, indicating an intermediate part, could fit the points equally well (i.e. rather poorly). The former option agrees with the ratio plots, and puts a lower limit on the electron density. In the latter case the density must be even higher, to produce lines that are all at least partially optically thick. More points are needed to decide which is the case.

HD 100546. Most lines in this CoG have a case B line strength ratio according to the ratio plots. These include Pfβ, Pfγ, Pfϵ and Pf11. Pfδ (fourth Pfund line from the left) is situated on top of a broader feature of the spectrum, usually attributed to polycyclic aromatic hy-

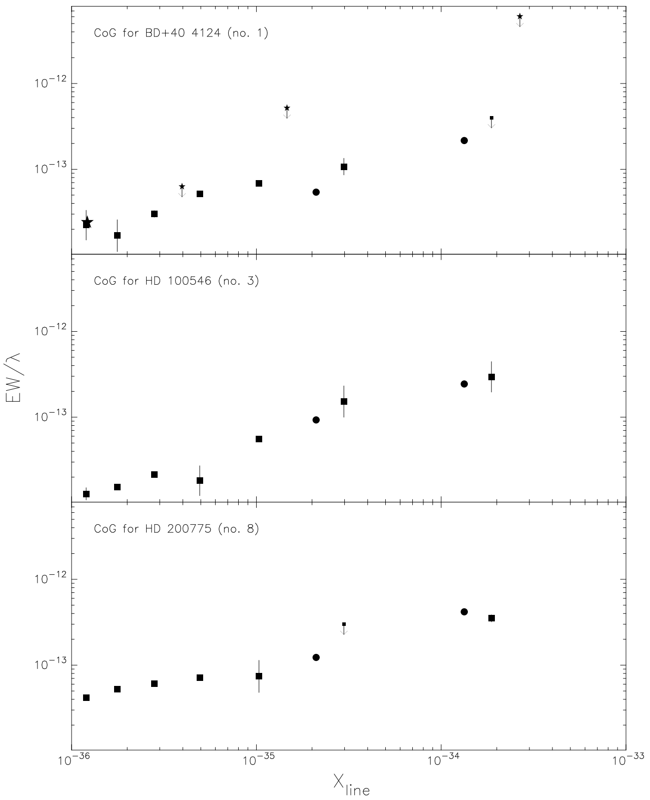

Fig. 7. Observational Curves of Growth of different sources. The symbols stand for different line series (□: Pfund, ∘: Brackett, ⋆: Humphreys). Smaller symbols with an arrow attached to it stand for upper limit measurements. The source number is printed with the name for easy comparison to other plots and tables.

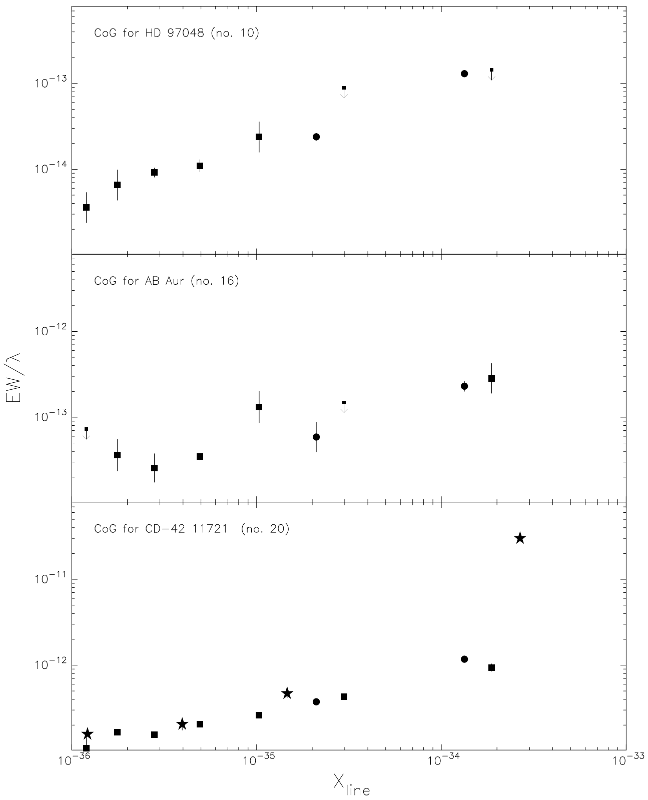

Fig. 8. Observational Curves of Growth. The symbols stand for different line series (□: Pfund, ∘: Brackett, ⋆: Humphreys). Smaller symbols with an arrow attached to it stand for upper limit measurements. The source number is again printed with the name for easy comparison to other plots and tables.

drocarbons (PAHs). Because of this feature the continuum under the line is difficult to measure. This could explain why this line has no case B line ratio. If one ignores the position of Pfδ, a straight line can be found for the Pfund series. Because the slope is less than one, the CoG does not shows an intermediate part, requiring a higher density to account for the observed optical depth effects.

HD 200775. The four leftmost Pfund lines have case B line ratios. However the slope suggested by all Pfund lines except Pfα is very flat. This would point to an almost optically thick part of the CoG. This would require a very dense structure, such as a dense disk. The position of Pfα is suggesting that the rightmost part of the plot slopes up. This could be because this line is coming from a nebula, and not from a disk. Such a nebula would not produce the lower lines, and only stick out above the flat part of the CoG at the higher lines. A similar trend is seen in the classical Be star γ Cas (see Hony et al. 2000).

HD 97048. Three Pfund lines have case B line ratios. These are the leftmost three lines. This CoG shows a straight line in the Pfund series with a slope of that is less than 1. This points to an intermediate part of the CoG that requires a considerable density.

AB Aur. The measurements of the lines in the spectrum of AB Aur have large error-bars because the spectrum is rather noisy. Because of these large error-bars no definite conclusion can be drawn about the shape of the CoG.

CD−42°11721. The 4 leftmost Pfund lines have case B line ratios. The Pfund series can be fitted to a straight line of slope ∼0.5. This points to the intermediate part of the CoG that requires a considerable density. The observed optical depth effects that cause the deviation of a slope = 1 linear plot are very strong.

4.4. Correlation with Stellar Luminosities

The presence of IR (and optical) H I lines in emission can either be the result of ionization and subsequent recombination of UV radiation of the central star, or it can be the result of some external process, such as accretion. If the IR (and optical) H I lines are driven by the UV radiation field of the central star, we expect a tight correlation between the total energy emitted by the central star in ionizing photons and the energy emitted in the H I lines. To check whether this is the case in our sample of Herbig Ae/Be stars, we calculate the stellar UV luminosities L_{UV} by fitting a Kurucz (1991) model to the (extinction corrected) spectral energy distribution of each star. Integrating over

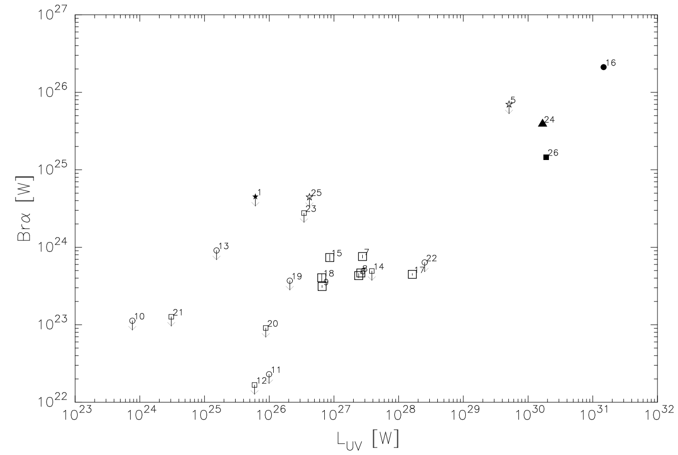

Fig. 9. UV - Brα Luminosity Correlation. Plot symbols have the same meaning as in Fig. 3. Note that these data are absolute (distance independent) values.

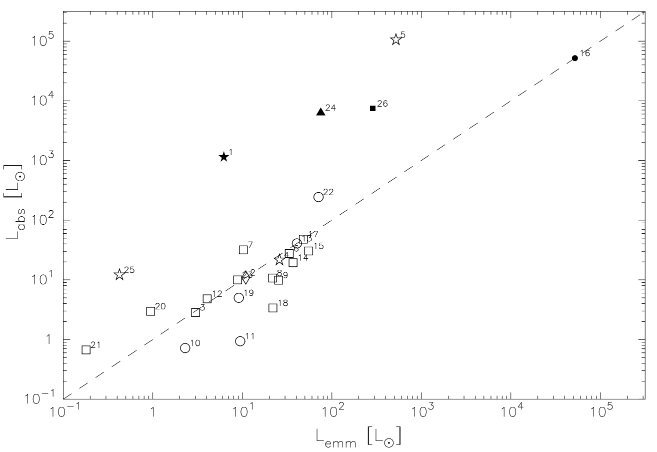

Fig. 10. Emitted vs Absorbed Energy for our programme stars. The dashed line is the 1:1 correlation line expected for a spherically symmetric envelope.

the UV part of the Kurucz model now gives the ultraviolet luminosity:

$$L_{UV} = 4\pi d^2 \int_{13.6eV}^{\infty} F_\lambda d\lambda \tag{4}$$

with F_λ the Kurucz model flux.

Brackett α is the most often detected IR line so we plot L_{UV} against this line (Fig. 9). A complete 1 to 1 correlation would signify that the IR lines are powered solely by the UV photons from the central star. The points in the upper right of the plot seem to correlate reasonably well with L_{UV}, but most sources concentrated in the middle of the plot and show limited variation in the Brα flux while the UV luminosity varies over a range of two orders of magnitude. We therefore conclude that for most sources in our sample, the IR H I lines do not seem to be driven by stellar UV photons.

The computed stellar luminosities can also be used to constrain the geometry of the circumstellar dust envelope. Using a similar approach as we used above to compute L_{UV} (but now over the entire wavelength range), we can compute the total amount of energy absorbed by dust particles, $L_{\rm abs}$, by subtracting the luminosity computed from a non-extinction corrected Kurucz model, fitted to the observed spectral energy distribution, to that computed from an extinction-corrected model. We can also compute the total amount of energy *emitted* by dust grains, $L_{\rm emm}$, by computing an integral over the (observed) infrared energy distribution in excess of the Kurucz model. For this computation, spectral interpolation between observed data points was done using a β spline under tension algorithm. Computed values of $L_{\rm abs}$ and $L_{\rm emm}$ for our programme stars are also listed in Table 1. They are extinction and distance corrected.

A reasonable correlation is visible when plotting $L_{\rm abs}$ against $L_{\rm emm}$ (Fig. 10). Most sources are concentrated just below the 1:1 line. For these correlating sources, reprocessing of UV photons from the central star is a sufficient energy source to power their infrared emission. Sources 1, 5, 24, 25 and 26 (respectively V376 Cas, Z CMa, BD+40°4124, PV Cep and HD 200775) deviate much from the 1:1 correlation line in Fig. 10. These sources could simply be deeply embedded and loose much of their energy to the general heating of the ISM. Alternatively, the presence of unseen companions may explain their deviating position in the $L_{\rm abs}$ vs. $L_{\rm emm}$ diagram.

4.5. Radio Continuum Emission

The radio continuum emission of our sources can also be used to gain information about the stellar environment. As described in section 3.2, radio continuum flux is mostly generated by free-free transitions in H-ions. Interactions between electrons and protons will also lead to recombinations. Hence a correlation is expected between the radio continuum flux and the H I recombination line strength. Using this expected correlation, Panagia (1991) showed that if the radio emission originates from a stellar wind one expects a linear relationship between the radio continuum flux and H I line emission.

Nisini et al. (1995) find a relation between the radio continuum emission coming from a stellar wind, using a simple wind model, and the Brα line. They assume Brα to be optically thick in their model. The final wind outflow velocity of the model is varied ($V_{\rm max}$ = 100–400 km s^{-1}) to produce a minimum and maximum value. Note that the correlation they predict can also be found using circumstellar disk models, and therefore is not conclusive to discern between the presence of a circumstellar disk or stellar wind.

In Fig. 11 the correlation is plotted between Brα and the 3.6 and 6.0 cm radio continuum emission. All sources detected at 6.0 cm, are also present in the 3.6 cm plot. One source is deviating strongly from model predictions and from the positions of most other stars. This is T Tau (source 3). Skinner & Brown (1994) found that the 3.6 cm radio continuum emission associated with the visible star is $\sim$ 1 mJy while the infrared source lying 0.6″ to the south

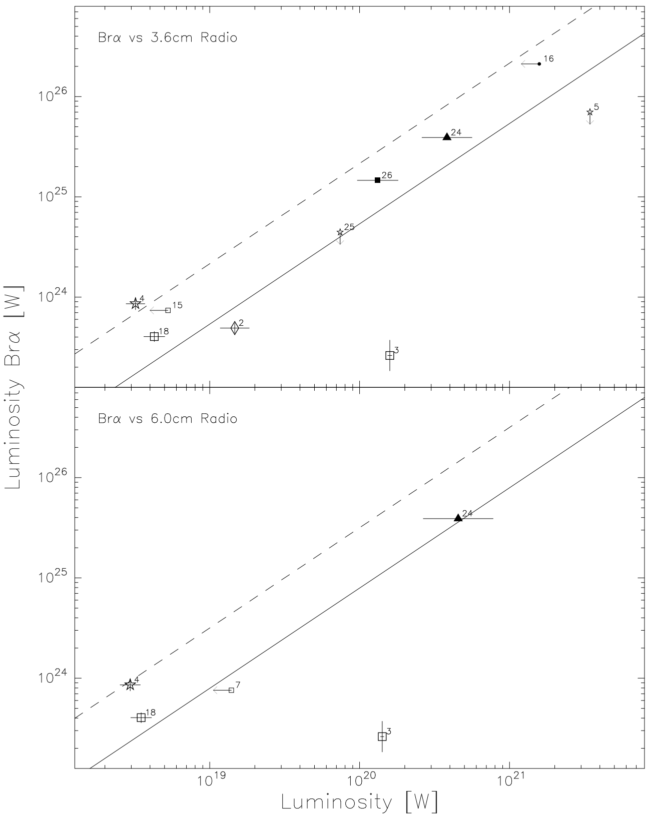

Fig. 11. Radio continuum vs Brα line flux. The top panel shows the continuum luminosity at 3.6 cm vs the Brα line luminosity, while the lower panel shows the same for sources with 6.0 cm measurements. Plot symbols have the same meaning as in Fig. 3. The solid and dashed lines are respectively the minimum and maximum wind model (Nisini et al. 1995) values. The numbers next to each symbol are the ID numbers that correspond to the ID numbers in various tables. Note that these data are absolute (distance independent) values.

of the visible star shows a flux of $\sim$ 5.5 mJy. In our plot the stronger source is plotted. The resulting difference in the corrected value of the radio luminosity if we substitute the lower value is almost 10 times less, shifting the point much closer to the model prediction.

From the plots of Brα vs the radio continuum emission it is clear that most stars show radio emission in line with model predictions. This shows that a stellar wind or circumstellar disk could be the origin of the observed lines. It rules out an extended H II region as the source of the IR emission lines.

5. Discussion

5.1. Circumstellar Geometry

From the tight correlation found between the Hα and Brα line fluxes, it can be concluded that the optical and infrared emission are coming from the same gas. Because of the high spatial resolution in the optical, this gas must be located close to the central star. Possible structures close to the central star from which the lines can be emitted are a stellar wind and/or a stellar disk.

For 14 sources the presence of a circumstellar disk is indicated by their Hα line profile (double-peaked). For 4 sources a P Cygni profile is seen, indicating a stellar wind. Note that a certain line profile does not rule out the existence of other structures in the star system. But these cannot dominate the shape of the Hα line profile.

5.2. Optical Depth

A detailed comparison between the ratio plots and the CoG analysis leads to an apparently contradictory result. While the CoG of all stars for which such a curve could be constructed suggests that all lines are (at least partially) optically thick, the ratio plots indicate that the higher numbers of the Pfund line series approach the case B, optically thin, limits.

However, the ratio plots of the Pfδ/Pfϵ etc. line flux ratios probe only a limited optical depth range. These ratio plots only measure the deviation from optically thin case B for a certain line ratio. Even if the ratio is case B, both lines could still be (partially) optically thick. In contrast, the CoG curves are very sensitive to optical depth effects since these curves measure the deviation from the optically thin limit over several transitions in the H-atom. We therefore conclude that most (if not all) of the lines we have detected are in fact (partially) optically thick.

In circumstellar environments densities that produce optically thick gas are found in stellar disks or very dense stellar winds. The more detailed view of the CoG shows that densities in our sources must be in the order of 10^7–10^9 cm^{-3}. Combined with the observation that the majority of sources show a double-peaked Hα profile it is likely that a stellar disk is present in the stellar surroundings of most Herbig Ae/Be stars.

5.3. Energy Source

With the exception of a few high UV luminosity sources, the IR recombination line fluxes do not seem to depend much on the amount of ionizing photons emitted by the central star. This could be caused by optical depth effects, where the IR emission is self-absorbed and therefore does not correlate with the UV luminosity. Another factor could be that the UV luminosity is not the only power source. Accretion luminosity (from material accreting onto the star from a circumstellar disk) could be another power source.

The presence of another power is also supported by the fact that in "classical" Be stars a sharp division exists between A and B stars: B stars show Hα emission, while A stars, often "shell" stars, do not show Hα emission. Apparently A stars do not have enough UV flux to power the circumstellar line emission. In our sample many stars have spectral type A or even F, while they do show many Balmer and IR H I lines in emission. This suggests that another mechanism is driving the H I line emission, possibly collisional ionization. This could also explain the presence of C IV and Si IV. These ions were found in Herbig Ae/Be stars by Bouret & Catala (1998), and cannot be ionized by the stellar UV radiation field.

5.4. Circumstellar Geometry

Stellar energy that is absorbed by a circumstellar dust particle can be reprocessed to infrared wavelengths and emitted there without a net contribution to the total flux. This kind of re-processing is done by passive envelopes. If on the other hand the envelope is contributing energy (e.g. due to viscous dissipation of energy by accretion) it is called active.

Sources that are positioned on the 1:1 line in Fig. 10 are consistent with a scenario in which energy from the central star is only reprocessed in a spherically symmetric, passive, circumstellar envelope. However, for the sources that are positioned below the 1:1 line, there is more emission than absorption. This suggests a disk symmetry, where some of the emitted energy can freely escape the system and a certain fraction (dependent on the inclination of the system) is absorbed by the disk.

Sources that are found above the 1:1 line have more absorption than emission. This could be a non-symmetric circumstellar envelope such as a circumstellar disk that is seen edge-on. In such a case a lot of the absorbed UV energy would be emitted in other directions than the line of sight, because an edge-on disk is very likely optically thick. This would then account for the lack of IR emission in stars that show a lot of UV absorption. If no correlation is found, the system could be active, have a non-symmetric envelope, or both. Usually, active systems have a greater $L_{\rm emm}$ than $L_{\rm abs}$, sometimes even greater than $L_{\star}$.

With the exception of the five deviating sources mentioned in section 4.4, which most likely have an active disk, most sources are positioned just below the 1:1 line in Fig. 10. On average there is therefore more emission than absorption. This suggests a disk symmetry, where some of the emitted energy can freely escape the system and a certain fraction (dependent on the inclination of the system) is absorbed in the disk.

5.5. Radio Correlation

The correlation between the radio emission and the IR line emission (together with the IR-optical correlation) pinpoints the radio source to the same emitting structure (close to the central star) as the IR and optical sources.

In the plot of Brα vs the 3.6 cm radio continuum emission 5 out of 6 sources show radio emission in line with model predictions for a stellar wind. However, we note that a model with similar velocities and spatial extent, in which the geometry is disk-like rather than wind-like, will predict the same relation between Brα and radio continuum flux. Therefore a (partially) ionized disk will be equally well able to explain the empirical relation between recombination line and radio continuum fluxes as a stellar wind.

What is ruled out by the radio correlation is an extended H II region as the source of the IR emission lines. And although both a disk and a wind could reproduce the observed radio continuum and the H I line fluxes, the Hα profiles of most of the stars do not show a wind-like (P Cygni) profile, suggesting that for most sources in our sample, the observed IR recombination lines arise in a circumstellar disk.

5.6. Remarks on Individual Sources

If we detected a whole series of IR H I lines in a single source, we were able to constructed a CoG. For these particular sources the conclusion found using the CoG can be supplemented by the other analytical tools we applied to our sample. In the following we describe the emerging picture for each of these stars.

BD+40°4124 (source 24) is a bright source that shows a complex Hα profile, which does not pinpoint to a single dominating structure in the circumstellar environment. The complexity of the profile could be caused by contributions from different structures. The correlation between the optical, IR and radio data show that these come from the same location in the circumstellar environment, close to the central star. In the HRD the source has a somewhat deviating position for a pre-main sequence (PMS) star because it is too luminous and thus above the birthline (see Fig. 1).

The CoG of this star indicates a high density is required to generate these optical depths. This could be situated in a circumstellar disk or stellar wind. The correlation between the UV luminosity and Brα points to the presence of an optically thin structure, such as a compact H II region. The ratio found in the $L_{\rm abs}$ vs $L_{\rm emm}$ plot is not anywhere near the 1:1 line. This points to an active and/or non-symmetric circumstellar envelope.

We conclude that BD+40°4124 has a complex circumstellar environment that could contain more than one dominating structure.

HD 100546 (source 8) shows a double-peaked Hα profile, that points to a circumstellar disk. The correlation between the optical and IR lines indicates that these lines come from close to the central star. No radio detection was available. This source has a position in the HRD typical for a PMS star.

The CoG of this source shows an intermediate part, that is partially optically thick. This points to a stellar wind or circumstellar disk. The position of HD 100546 in the UV luminosity vs Brα plot is not conclusive. From the $L_{\rm abs}$ vs $L_{\rm emm}$ plot it is clear that HD 100546 has more emission than absorption. This suggests a disk geometry.

We conclude that HD 100546 has a circumstellar disk and does not show evidence for other circumstellar structures.

HD 200775 (source 26) is a bright source that shows a double-peaked Hα profile, which points to a circumstellar disk. The correlation between the optical, IR and radio data show that these come from the same location in the circumstellar environment, close to the central star. In the HRD the source has a somewhat deviating position for a pre-main sequence (PMS) star because it is too luminous and thus above the birthline (see Fig. 1). Possibly this massive (10 $M_\odot$) young star is starting its evolution off the zero-age main-sequence.

The CoG of this source shows a slope that is almost flat. This could be the (almost) optically thick part of the CoG. Such a CoG requires a high density, as is most likely to be found in a circumstellar disk. The CoG slopes up towards the right. This is probably because this line is receiving extra contribution from an additional lower density component near the star, such as a nebula.

Evidence for such a nebula is also seen in the correlation between the UV luminosity and Brα. The ratio found in the $L_{\rm abs}$ vs $L_{\rm emm}$ plot is not anywhere near the 1:1 line. HD 200775 has much more absorption than emission. This points to an active and/or non-symmetric circumstellar envelope.

We conclude that HD 200775 has a complex circumstellar environment that contains a circumstellar disk, and probably also a compact H II region.

HD 97048 (source 7) shows a double-peaked Hα profile, that points to a circumstellar disk. The correlation between the optical and IR lines indicates that these lines come from close to the central star. No radio detection was available. This source has a position in the HRD that is typical for Herbig Ae/Be stars.

The CoG of this source shows a slope that is not much less than 1, indicating the beginning of the intermediate part of the CoG, where optical depth effects are just beginning to show.

We find that HD 97048 shows no correlation in the UV luminosity vs Brα plot. This points to an optically thick disk or another source of line excitation. The IR recombination lines are not driven by stellar UV photons. The ratio found in the $L_{\rm abs}$ vs $L_{\rm emm}$ plot is just above the 1:1 line. It has a bit more absorption than emission. This could be because of a (somewhat) active disk.

We conclude that HD 97048 might have a circumstellar disk and does not show evidence for other circumstellar structures.

CD$-$42°11721 (source 16) is a bright source that shows a single-peaked Hα profile, which suggests the gas is not moving parallel to the line of sight. The correlation between the optical and IR lines indicates that these lines come from close to the central star. No radio detection was available. In the HRD the source has a deviating position for a pre-main sequence (PMS) star because it is too luminous and very hot, and thus of very early spectral type, located far above the birthline.

The slope of the CoG is $\sim$0.5 which is in the intermediate part of the CoG, with pronounced optical depth effects. The correlation between the UV luminosity and Brα points to the presence of an optically thin structure, such as a H II region. The ratio found in the $L_{\rm abs}$ vs $L_{\rm emm}$ plot is 1. This suggests a spherical symmetry. This could be a stellar wind or certain specific inclinations of a circumstellar disk. The energy in this system is only reprocessed by this spherically symmetric envelope.

We conclude that CD$-$42°11721 has a circumstellar environment that likely contains a circumstellar disk. Also a wind or compact H II region is possibly present.

6. Concluding Remarks

Our results can be summarized as follows:

1. The correlation between Hα and Brα suggests that the principal IR line emission is coming from a compact region close to the central star. This could be a disk and/or wind. The radio emission is also shown to correlate with the IR lines, locating the radio source also close to the central star. This result confines the possible circumstellar structures to a disk or a wind.
2. The majority of stars have a double-peaked Hα profile which indicates the gas is in a rotating geometry, typical for a disk.
3. The CoG indicates that the IR recombination lines are (partially) optically thick. Similar optical depths are expected for the sources where we could not construct a CoG, based on the optically thick Brα and Pfα lines found in the ratio plots. The emitting gas must be dense enough to produce optically thick IR lines. Most likely this is a stellar disk.
4. We find no strong correlation between the UV luminosity of the central star and the strength of the H I recombination lines. This suggests that the H I lines are not emitted by gas in a radiatively driven stellar wind. The observations are consistent with gas in a disk, ionized partly by the radiation of the central star and possibly by other sources of energy, such as an accretion-generated feature.
5. The correlation between the absorbed and emitted energy in most sources is just below the 1:1 line, with a bit more emission than absorption. For these correlating sources the stellar UV energy is only reprocessed. This could be a passive circumstellar disk.

We conclude that the combination of the evidence from these five conclusions strongly suggest that a circumstellar disk is present in many if not all Herbig Ae/Be stars. This disk, dense enough to contain (at least) partially optically thick gas, is the main contributor to the IR H I emission lines observed by ISO. Besides the central star, another source of energy (e.g. accretion) is required to power the IR H I lines.

Acknowledgements. This research has made use of the Simbad data base, operated at CDS, Strasbourg, France. LBFMW acknowledges financial support from an NWO *Pionier* grant.

References

Abt H.A., Morrell N.I., 1995, ApJS 99, 135
Anglada G., Rodriguez L.F., Canto J., Estalella R., Torrelles J.M., 1992, ApJ 395, 494
Baade D., Stahl O., 1989, A&A 209, 268
Bernasconi P.A., 1996, A&AS 120, 57
Beskrovnaya N.G., Pogodin M.A., Shcherbakov A.G., Tarasov A.E., 1994, A&A 287, 564
Beskrovnaya N.G., Pogodin M.A., Yudin R.V., Franco G.A.P., Vieira S.L.A., Evans A., 1998, A&AS 127, 243
Böhm T., Catala C., 1993, A&AS 101, 629
Böhm T., Catala C., 1995, A&A 301, 155
Bouret J., Catala C., 1998, A&A 340, 163
Cohen M., Kuhi L.V., 1979, ApJS 41, 743
Cohen M., Kuhi L.V., 1980, S&T 59, 373
Cohen M., Kuhi L.V., Spinrad H., Harlan E.A., 1981, ApJ 245, 920
Corcoran M., Ray T.P., 1998, A&A 331, 147
de Graauw Th., Haser L.N., Beintema D.A., et al., 1996, A&A 315, L49
de Winter D., Thé P.S., 1990, Ap&SS 166, 99
di Francesco J., Evans N.J., Harvey P.M., et al., 1997, ApJ 482, 433
Dunkin S.K., Barlow M.J., Ryan S.G., 1997, MNRAS 286, 604
Dunkin S.K., Barlow M.J., Ryan S.G., 1997b, MNRAS 290, 165
Elias J.H., 1978, ApJ 224, 857
Férnandez M., Ortiz E., Eiroa C., Miranda L.F., 1995, A&AS 114, 439
Finkenzeller U., Mundt R., 1984, A&AS 55, 109
Fluks M.A., Plez B., Thé P.S., et al., 1994, A&AS 105, 311
Grady C.A., Pérez M.R., Talavera A., et al., 1996, A&AS 120, 157
Gray R.O., Corbally C.J., 1998, AJ 116, 2530
Grinin V.P., Thé P.S., de Winter D., Giampapa M., Rostopchina A.N., Tambovsteva L.V., van den Ancker M.E., 1994, A&A 292, 165
Güdel M., Benz A.O., Catala C., Praderie F., 1989, A&A 217, L9
Hillenbrand L.A., Meyer M.R., Strom S.E., Skrutskie M.F.: 1995, AJ 109, 280
Hony S., Waters L.B.F.M., Zaal P.A., et al., 2000, A&A 355, 187
Houk N., Cowley A.P., 1975, "Michigan Catalogue of two-dimensional spectral types for the HD star". Ann Arbor: University of Michigan, Department of Astronomy, 1975
Kenyon S.J., Dobrzycka D., Hartmann L., 1994, AJ 108, 1872
Kessler M.F., Steinz J.A., Anderegg M.E., et al., 1996, A&A 315, L27
Kurucz R.L., 1991, in *"Stellar atmospheres–Beyond classical models"* (eds. A.G. Davis Philip, A.R. Upgren, K.A. Janes), L. Davis press, Schenectady, New York, p. 441
Maihara T., Kataza H., 1991, A&A 249, 392
Malfait K., Bogaert E., Waelkens C., 1998, A&A 331, 211
Mannings V., Sargent A.I., 1997, ApJ 490, 792
Marraco H.G., Rydgren A.E., 1981, AJ 86, 62
Meeus G., Waelkens C., Malfait K., 1998, A&A 329, 131
Menzel D.H., Baker J.G., 1938, ApJ 88, 52
Miroshnichenko A.S., Mulliss C.L., Bjorkman K.S., et al., 1998, PASP 110, 883
Nisini B., Milillo A., Saraceno P., Vitali F., 1995, A&A 302, 169
Panagia N., 1991, "NATO ASI: Physics of Star Formation and Early Stellar Evolution". Dordrecht, Kluwer
Pérez M.R., Grady C.A., 1997, Sp. Sci. Rev. 82, 407
Pogodin M.A., 1994, A&A 282, 141
Praderie F., Catala C., Czarny J., Thé P.S., Tjin A Djie H.R.E., 1991, A&AS 89, 91
Pugach A.F., 1988, Astrofizika 29, 448
Reipurth B., Pedrosa A., Lago M.T.V.T., 1996, A&AS 120, 229
Rogers C., Heyer M.H., Dewdney P.E., 1995, ApJ 442, 694
Shevchenko V.S., Ezhkova O.V., Ibrahimov M.A., van den Ancker M.E., Tjin A Djie H.R.E., 1999, MNRAS 310, 210
Shevchenko V.S., Ibragimov M.A., Chenysheva T.L., 1991, SvA 35, 229
Shevchenko V.S., Yakubov S.D., 1989, A. Zh. 66, 718
Shore S.N., Brown D.N., Bopp B.W., et al., 1990, ApJS 73, 461
Skinner S.L., Brown A., 1994, AJ 107, 1461
Skinner S.L., Brown A., Stewart R.T., 1993, ApJS 87, 217
Slettebak A., 1966, ApJ 145, 121
Storey P.J., Hummer D.G., 1995, MNRAS 272, 41
Thé P.S., de Winter D., Pérez M.R., 1994, A&AS 104, 315
Tjin A Djie H.R.E., Thé P.S., Andersen J., et al., 1989, A&AS 78, 1
van den Ancker M.E., de Winter D., Tjin A Djie H.R.E., 1998, A&A 330, 145
van den Ancker M.E., Bouwman J., Wesselius P.R., Waters L.B.F.M., Dougherty S.M., van Dishoeck E.F., 2000, A&A 357, 325
Voshchinnikov N.V., 1981, Astron. Tsirk. 1200, 1
Waters L.B.F.M., Waelkens C., 1998, ARA&A 36, 233
Whitcomb S.E., Gatley I., Hildebrand R.H., et al., 1981, ApJ 246, 416
Whittet D.C.B., Kirrane T.M., Kilkenny D., et al., 1987, MNRAS 224, 497
Zaal P.A., Waters L.B.F.M., Marlborough J.M., 1995, A&A 299, 574
Zinnecker H., Preibisch T., 1994, A&A 292, 152